J/ψ and $\psi(2S)$ production in p+p collisions at $\sqrt{s} = 500$ GeV at STAR experiment

Qian Yang(USTC)

June 3, 2017

Contents

Chapter 1

J/ψ analysis

1 Data sets and triggers

In this analysis, we reconstruct high p_T J/ψ and $\psi(2S)$ in the High Tower(HT) trigger events via di-electron channel. The trigger name, trigger definition and sampled luminosity are listed in Table 1. The bandwidth limitation is the main constraint for data taking, normally, prescaled technical was used for BHT triggered events. At the end of the runs, a pre-scale about two was applied, so only a fraction of the events satisfying BHT1 triggers can be recorded. The data was produced in the production series P11id using SL11d library. Figure 1 is the BHT1 Integrated luminosity as a function of time.

2 Event selection

The importance of the vertex-finding algorithm to find a real trigger event is self-evident. In p+p collisions, the low charged-particle multiplicity and high luminosity, which results in a pile-up rich collision environment, are an all set obstacle to finding the truth vertex. The charged-particle multiplicity is shown in left panle of Figure 1.2. A PPV vertex finer (Pile-up Protected Vertex finder) is used in the data. The PPV, which finds the Z position of a vertex, requires a beam-line constraint to determine the X and Y values of the vertex. The beam

Table 1.1: Run11 500GeV p+p BHT1 triggers

Trigger Name	Trigger Threshold	Number of Events	Sampled Luminosity
BHT1	E_T >4.3 GeV	154M	22 pb^{-1}

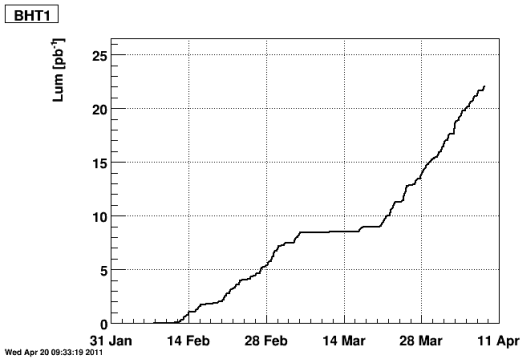

Figure 1.1: BHT1 Integrated luminosity as a function of time

Table 1.2: Event selection in run11 500GeV p+p BHT1 trigger

Event Cut Parameters	Cut Value
Trigger Id	320501
Valid vertex	$V_x(TPC) > 10^{-5}cm$ or $V_y(TPC) > 10^{-5}cm$ or $V_z(TPC) > 10^{-5}cm$
V_z	$\|V_z(TPC)\| < 200cm$

line constraint is calculated by fitting high multiplicity events with Minuit VF without any constraints on the vertex position. A straight line is fit to the vertex distributions to obtain a relationship among x, y, and z. This method will give a correct vertex, we take the highest ranking vertex in every event as our event primary vertex. A valid vertex requirement, 3 components of the reconstructed vertex positions not simultaneously below 10^{-5} cm. is applied too. Figure 1.2 right panel is the V_x vs.V_y distribution, the beam line is clearly shown. Figure 1.3 shows the V_z distribution. All of the cuts on event level for the triggers are summarized it Table 2.

3 Track selection and electron identification

To ensure a good track reconstruction in TPC, several requirements are placed on tracks. Number of reconstruction hit points (nHitsFit) which represent the number of hits used to reconstruct track's transverse momentum can have a maximum of 45 hits for global track and 46 for a primary track. To ensure a good track without track splitting effects, nHitsFit needs to be larger than 25. The number of dE/dx hit points (nHitsDedx) which used to calculate the particle ionization energy loss per unit length(dE/dx) in the TPC, needs to large than 15 for a good dE/dx resolution requirement. Taking TPC coverage

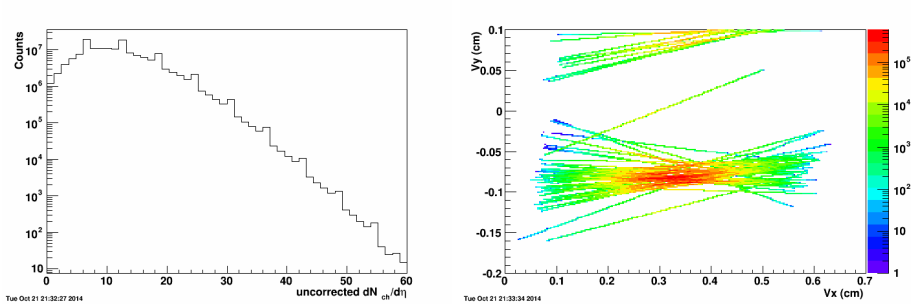

Figure 1.2: left: charged-particle multiplicity in p+p 500 GeV, right: primary vertex V_x v.s. V_y distribution

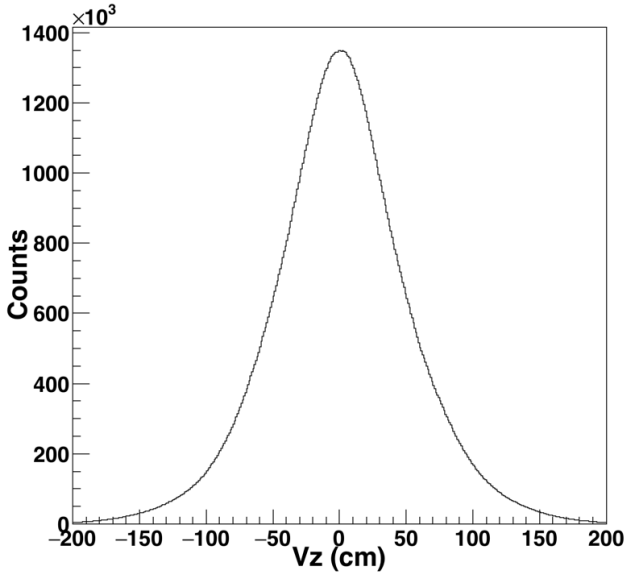

Figure 1.3: V_z distribution from BHT1 triggered events

Table 1.3: Primary track selection in p + p collisions

Event Cut Parameters	Cut Value
Pseudorapidity	$\|\eta\| < 1.0$
Spatial Hits	$nHitsFit \geq 25$
dE/dx Hits	$nHitsDedx \geq 15$
dca	$dca > 3cm$ or $dca > 1cm$

into account, each track required in eta range of $|\eta| < 1$.
Since J/ψ has a very small decay length, when we selection tracks, we actually more interesting in primary tracks with a small DCA value. The DCA is distance of closest approach(DCA) to the event primary vertex of its associated global track. In this analysis, the DCA cut have several consider:1) reject pile-up track, since there are a lot of pile-up tracks in event, 2) reject the tracks from long decay length particle, such as K_s, λ and etc, 3) tracks from differ enter primary vertex. Furthermore, for those triggered BTOW tracks or could match with BEMC, which we called "EMC+TPC" electron, it would have a relative higher transverse momentum. When it goes through the detector multi-scatting would have less effect on it. All these consider required a small DCA value. So DCA less than 1 cm cut is required for "EMC+TPC" electron. Those tracks do not match with EMC, we apply a DCA less than 3 cm cut. The track quality requirements for "EMC+TPC" electron and "TPC" electron are lists in Table 1.3.

3.1 dE/dx

Charged particles, while traversing through the TPC gas volume, will interact with the gas atoms and lose energy by ionizing electrons out of the gas atoms. This specific ionization energy loss called dE/dx is a function of particle's momentum magnitude. This property provides a strong particle identification power when select electron candidates. The ionization energy loss by charged particles in material is given by Bethe-Bloch formula. As for thin material, it is described by the more precise Bichsel formula. With the measured particle momentum and dE/dx, the particle type can be determined by comparing the measurements against the Bichsel expectation. However, a particle with certain momentum, the dE/dx distribution at length L is a Landau distribution rather than a Gaussian distribution. Thus a new variable is used in order to have a proper deconvolution of dE/dx into a Gaussians distribution. $n\sigma_e$ is used to identify electrons. $n\sigma_e$ defined as the dE/dx normalized to the expected dE/dx for electrons obtained from the Bichsel functions($dE/dx_{Bichsel}$), also scaled by

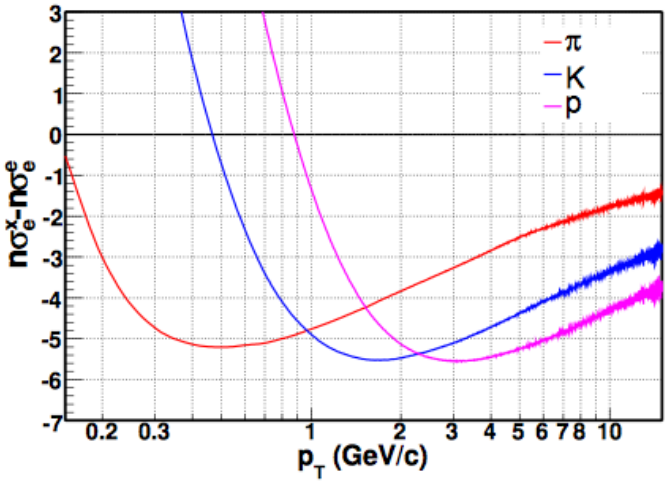

Figure 1.4: Expected $n\sigma_e$ distribution for electron and charged hadrons(π, K, p)

the dE/dx resolution($\sigma_{dE/dx}$). as showed in formula.

$$n\sigma_e = \frac{1}{\sigma_{dE/dx}} log(\frac{dE/dx_{Measured}}{dE/dx_{Bichsel}})$$

Figure 1.4 shows the expected $n\sigma_e$ distribution for electron and charged hadrons(π, K, p). However, due to imperfect dE/dx correction, the real measured mean and width of the $n\sigma_e$ distribution are not exactly equal to 0 and 1, as shown in Figure 1.5 and Figure 1.6. The electron sample are from phonetic electron.

$n\sigma_e$ could also describe the deviation of measured dE/dx value from the prediction value. Figure 1.7 shows the $n\sigma_e$ verse momentum distribution. Two cores are showed, the core appeared around $n\sigma_e \sim -3$ is dominated charged hadron, while the core appeared around 0 is the electron candidates. In this analysis, both electron candidates with a $|n\sigma_e| < 2$ are utilized.

3.2 BEMC p/E

High energy electron and high energy hadron pass through a material, especially an electromagnetic absorber has a very different phenomenon. The BEMC towers with 30 radiation lengths are thick enough to collect all energy of an electron produced during the collisions. So for electrons their momentum-to-energy ratio $p/E \sim 1$, while for high-energy hadron, a large part of high

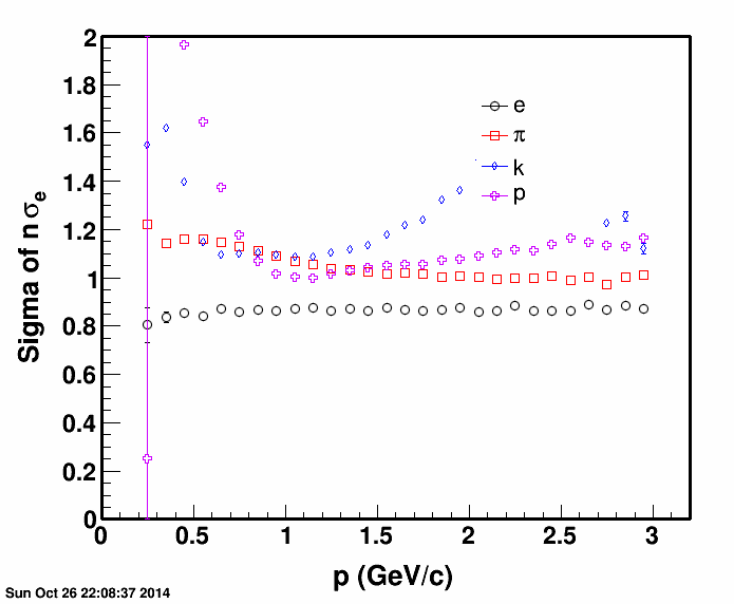

Figure 1.5: Electron $n\sigma_e$ width value as a function of momentum

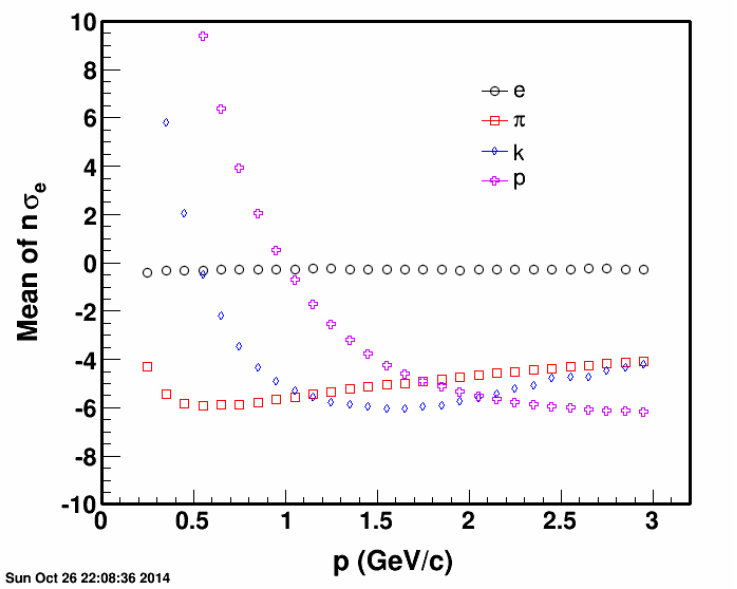

Figure 1.6: Electron $n\sigma_e$ mean value as a function of momentum

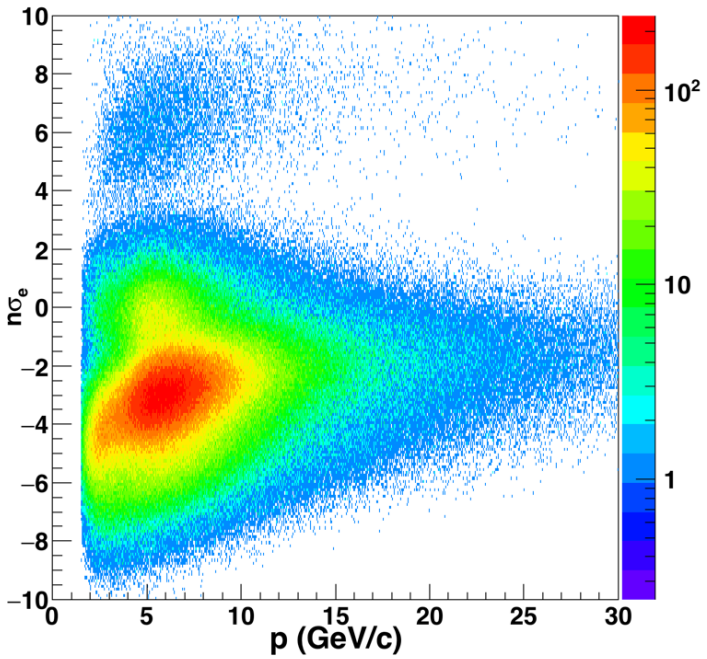

Figure 1.7: Track $n\sigma_e$ vs. p_T after all track quality cuts

energy hadrons are so-called "Minimum Ionizing Particles"(MIP). These particles deposit very litter energy in the calorimeter. The rest part of particles may interaction with nuclei via strong interaction, which additionally deposes some energy in BEMC. So for high energy hadrons the p/E distribution will have a very broad distribution. This helps to suppress the hadron and enhance election sample purity.

To compare the electron and hadron p/E distribution, we used $n\sigma_e < -2$ to get a hadron rich sample. Electron rich sample is obtained by using different cut in different p_T range. At middle p_T range, $n\sigma_e$ information from TPC and $1/\beta$ information from TOF is used. At high p_T range, a tighter $n\sigma_e$ is used. The distribution for electron rich sample and hadron rich sample are showed in Figure 1.8, hadron sample is scaled to the same number of events as electron rich sample. For electron rich sample, its peak at ~ 1 and shows almost a Gaussian distribution. However, the hadron sample has a long tail on the right-hand side. We cut on p/E between 0.3 and 1.5 to select electrons for the high-p_T J/ψ analysis.

In the spectra measurement, it is important to ensure the J/ψ decay electron fired the trigger, an adc0 cut method was proposed by Purdue group to select a trigger electron. The details can be found at STAR Analysis Note PSN0522:"High p_T Non-photonic Electron Production in p+p collisions at $sqrts =$

Table 1.4: The summary of the electron identification cuts

Parameter	"EMC+ TPC electron"	"TPC" electron
p_T	$p_T > 3.5 GeV/c$	$p_T > 1.0 GeV/c$
Pseudorapidity	$\|\eta\| < 1.0$	$\|\eta\| < 1.0$
Spatial Hits	$nHitsFit \geq 25$	$nHitsFit \geq 25$
dE/dx Hits	$nHitsDedx \geq 15$	$nHitsDedx \geq 15$
dca	$dca > 1cm$	$dca > 1cm$
$n\sigma_e$	(-2,2)	(-2,2)
p/E	(0.3, 1.5)	
adc0	> 290	

$200 GeV$". The adc0 value of the triggered electron is large than 290, which correspond to the online $dsmadc > 18$ cut.

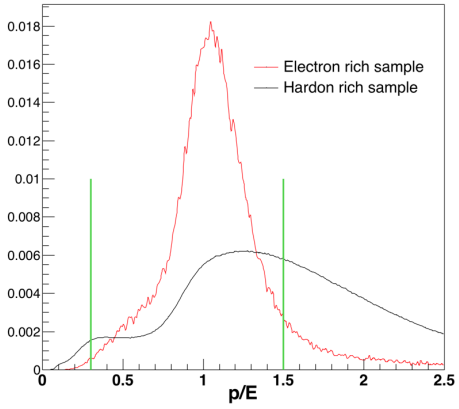

Figure 1.8: The pc/E distribution for hadron rich and electron rich sample from the same data set.

4 Electron candiates

With discussion above, Table 1.4 shows the summary of the electron identification cuts.

5 High-p_T J/ψ reconstruction

Electrons pairs that originated from the the same collision vertex have been used to reconstruct the di-electron invariant mass spectrum. We paired

"EMC+TPC" electrons with "TPC" electrons which has a relative low transverse momentum and also pair "EMC+TPC" with "EMC+TPC" electrons. A track ID index is used to avoid the double counting. The unlike-sign pairs($e^+ + e^-$) spectrum contained the real J/ψ signal, random combinations of opposite-sign pairs and contribution from some correlated background. Like-sign pairs($e^+ + e^+$ and $e^- + e^-$) have been used to estimate the background from random combinations of opposite-sign pairs. Normally, the number of background pairs, $N_{Like-Sign}$ is calculated as:

$$N_{Like-Sign}(m) = 2 \times \sqrt{N_{e^+e^+}(m) \times N_{e^-e^-}(m)}$$

where N is the number of like-sign pairs. However, the electron candidate statistics are very low in p+p event. There are large possibility that $N_{e^+e^+}$ or $N_{e^-e^-}$ equal to 0. Then, the formula may not reproduce the combinatorial background reasonably and thus underestimate the combinatorial background. So here we use the sum of $N_{e^+e^+}$ and $N_{e^-e^-}$ instead of 2 times of their geometrical mean as the combinatorial background. Figure 1.9 shows the J/ψ signal within $|y| < 1$. The unlike-sign and unlike-sign background are also shown, a J/ψ peak are clearly showed at around $3.1 GeV/c^2$. On the left-hand side of the J/ψ peak, a tail is shown which is mainly from electron's bremsstrahlung along its path caused. So we extracted raw yield by counting the unlike-sign and like-sign pairs in the mass range from 2.7 to 3.3 GeV/c^2. The amount of background is quantified by using the signal-to-background ratio, S/B, where $S = N_{J/\psi} = N_{+-} - N_{Like-Sign}$ and the background is $N_{Like-Sign}$. The signal strength is defined by its significance, $S/\sqrt{S+B}$. we have about 9000 raw J/ψ signal, with an S/B ratio of 1.2 and signal strength of 58.6 in this dataset.

The J/ψ is divided into 19 p_T bins with different bin width as shown in Figure 1.10. After the background subtraction, some residual background contributions from $c\bar{c}$, $b\bar{b}$ and Drell-Yan need to be further subtracted.

6 Acceptance and efficiency

In p+p collisions, the Multiplicity is relative low as showed in Figure 1.2. Each event embedded in 5 J/ψs, equivalent 10 tracks, this may have an effect on the TPC reconstruction efficiency. This effect has been studied by Bingchu Huang, who embedded 15 Pions into a 200GeV p+p event, his study shows less than 0.3% in efficiency difference, showed in Figure 1.11. Detail can be found in his presentation.

Multiple electron in the same p+p event may enhance the electron trigger efficiency, especially at low p_T. In some case. Two or more electrons can hit on the same BEMC tower, this tower obviously has a higher deposited energy than

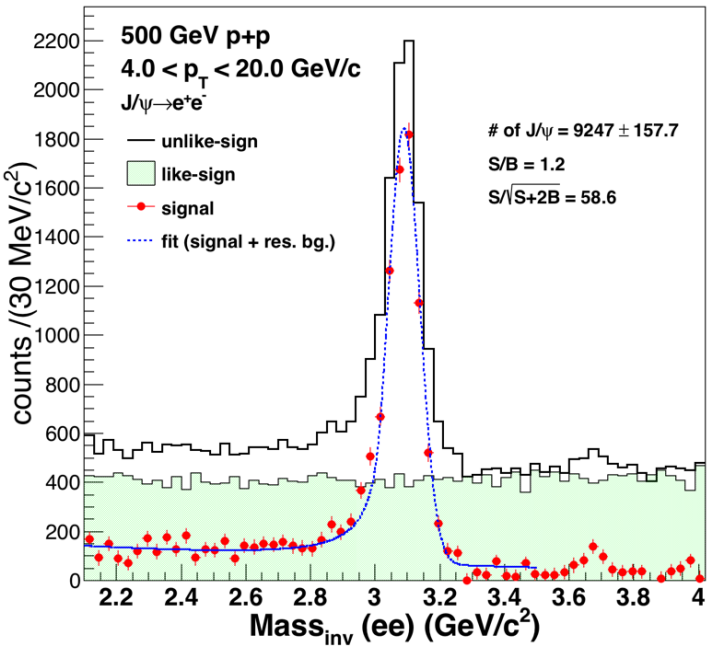

Figure 1.9: dielectric invariant mass

a single electron. Figure 1.12 shows the correlation of two BHT1 triggered MC electrons. The x-axis is the reconstructed p_T of the lower p_T electron. The y-axis is $dR = \sqrt{\Delta y_{MC}^2 + \Delta\phi_{MC}^2}$. A band at low p_T and small dR range benefited from such a multi-hit is clearly seen. This kind of trigger benefit effect will have a very large impact for low p_T electron. To get rid of this trigger benefit effect, an isolation cut on the embedded electrons, are applied. we reject those two electrons if they are satisfy $|\Delta y_{MC}| < 0.1$ or $|\Delta\phi_{MC}| < 0.5$. After applied the cuts, the $\Delta\phi_{MC}$ v.s. Δy_{MC} distribution and the p_T^{MC} vs. y^{MC} distribution are showed in Figure 1.12, also the dR vs p_{Tlow} are showed in Figure 1.12. The band is removed successfully.

The input MC$J/\psi$ p_T, ϕ and rapidity distribution are shown in Figure 1.13. Trigger efficiency is an essential part of the embedding. Figure **??** shows the comparison between embedding and data, the edges due to trigger cut matched very well, which means: 1) the trigger implementation is quite good; 2) the energy scale of BEMC is very well.

The momentum resolution and bremsstrahlung radiation energy loss are also obtained from the embedding. We separate them into different transverse momentum p_T bins. Figure 1.15 shows the ratio of reconstructed p_T and MC p_T, p_T^{RC}/p_T^{MC}, distributions in different p_T bins. The long tails on the left side are contributed by bremsstrahlung radiation energy loss. A strong p_T dependence

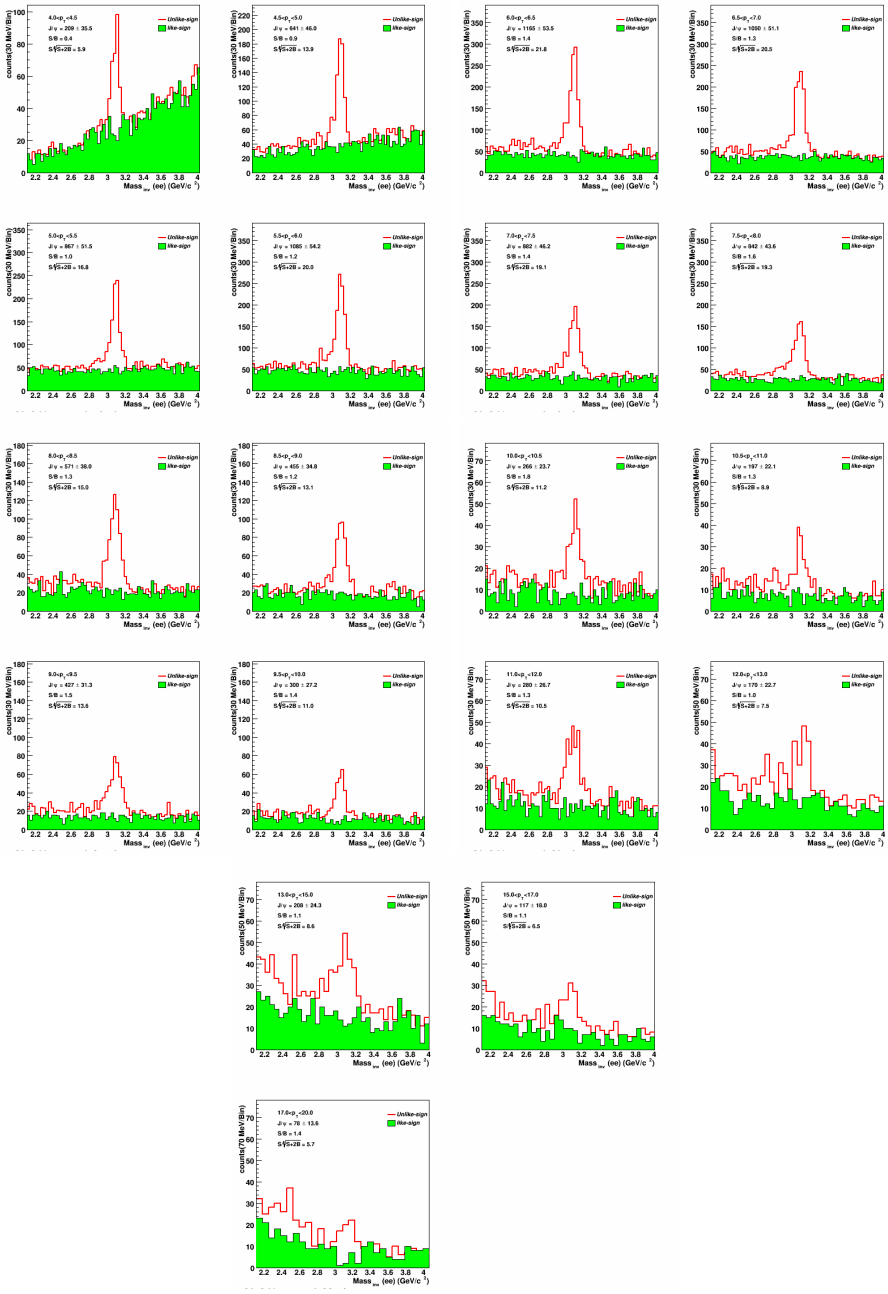

Figure 1.10: dielectric invariant mass in p_T

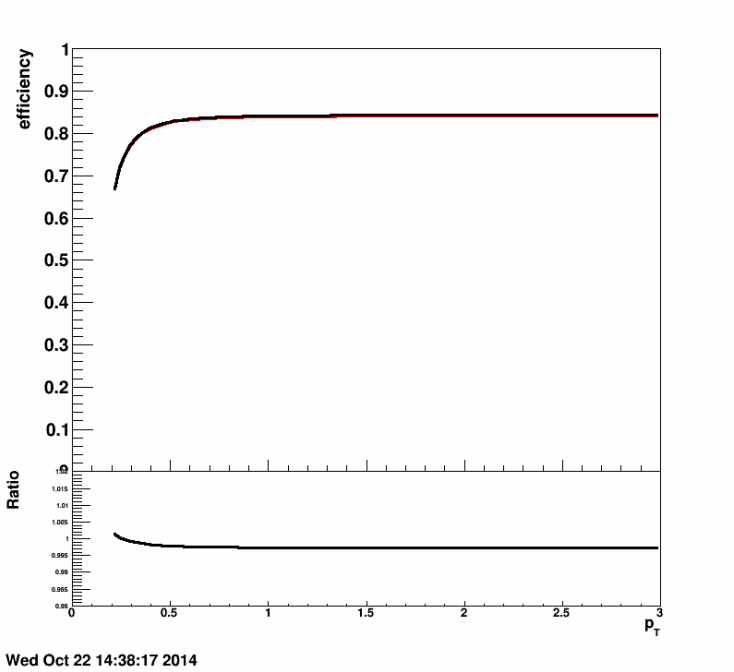

Figure 1.11: The embedding efficiency change

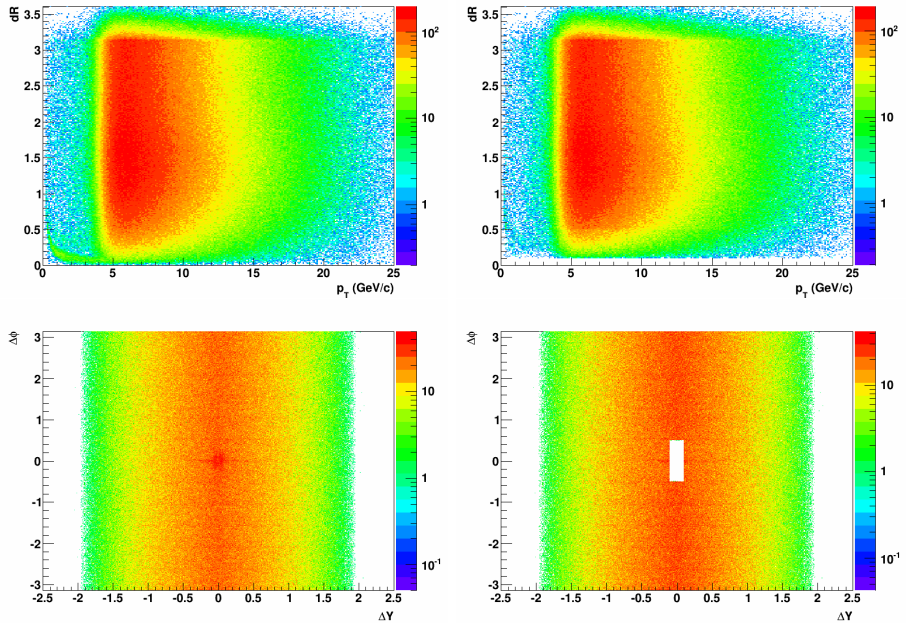

Figure 1.12: The correlation of two BHT1 triggered MC electrons, left before dR cut, right after dR cut.

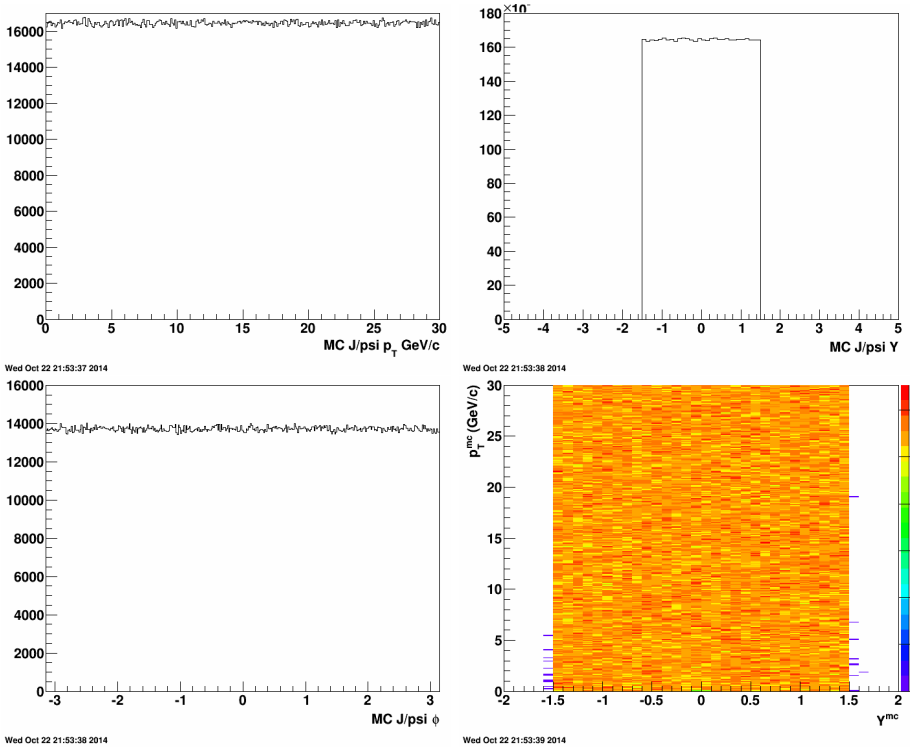

Figure 1.13: input MC J/ψ p_T, Rapidity, Phi and p_T vs Rapidity distribution

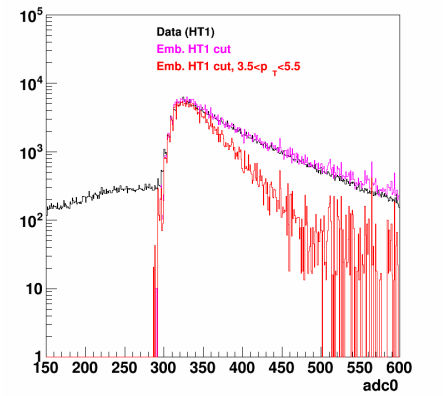

Figure 1.14: The adc0 distributions for electrons from embedding compared to the distributions from real data.

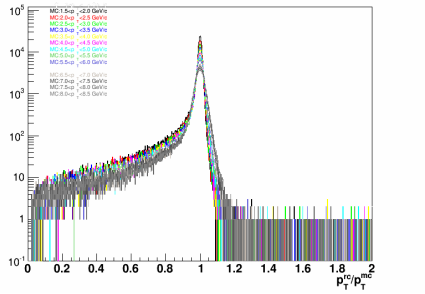

Figure 1.15: p_T^{RC}/p_T^{MC} distributions for electrons in different p_T bins within $|\eta| < 1$.

is shown.

$n\sigma_e$ cuts efficiency

We get the $n\sigma_e$ distribution from data. After enhancing the electron contribution in the $n\sigma_e$ distribution by using TOF and selecting photonics electrons, As showed in Figure 1.6 and Figure 1.5, the $n\sigma_e$ width and mean distribution as a function of p_T, the width is about 0.9 and the mean value is 0. Thus the $nsigma_e$ cut efficiency is larger than 95%.

nHitsDedx cut efficiency

For nHitsDedx cut efficiency, we compared the number of tracks with and without this cut after the basic tracking quality cuts as we used in this analysis. This efficiency the average is about 97%.

7 Yield extraction and total efficiency

7.1 Yield extraction

As shown in Figure 1.9, with combinatorial background subtracted, residual background from $c\bar{c}$, $b\bar{b}$ and Drell-Yan need to be further subtracted. In this analysis, we use an exponential function to describe the residual background. To evaluate the mass window cut efficiency and account for electron radiative energy loss(Bremsstrahlung), the J/ψ line shape is obtained from MC J/ψ. We fit MC J/ψ signals by Crystal-Ball function which is consists of a Gaussian core portion and a power-low low-end tail below a certain threshold. Such a power-low tail is account for the energy loss in material. The Function is given by:

$$f(x;\alpha;n;\overline{x};\sigma) = N \cdot \begin{cases} exp(-\dfrac{(x-\overline{x})^2}{2\sigma^2}), & \dfrac{x-\overline{x}}{\sigma} > -\alpha; \\ A \cdot (B - \dfrac{x-\overline{x}}{\sigma})^{-n}, & \dfrac{x-\overline{x}}{\sigma} \leq -\alpha \end{cases}$$

where :
$A = \frac{n}{|\alpha|}^n \cdot exp(-\frac{|\alpha|^2}{2})$
$B = \frac{n}{|\alpha|} - |\alpha|$
$C = \frac{n}{|\alpha|} \cdot \frac{1}{n-1} \cdot exp(-\frac{|\alpha|^2}{2})$
$D = \sqrt{\frac{\pi}{2}}(1 + erf(\frac{|\alpha|}{\sqrt{2}}))$
$N = \frac{1}{\sigma(C+D)}$

In the fitting procedure, we need to release σ as a free parameter in order to deal with the imperfect momentum simulation. After fitting, the residual

background is obtained by integrating the exponent function in the mass range of 2.7 $\sim$ 3.3 GeV/c^2. The mass counting efficiency is corrected by using the Crystal ball function line shape. The mass cuts efficiency as a function of p_T is almost constant as you can see from Figure 1.16, the first point has a large deviation is due to poor statistics, when we correct the mass cut efficiency in this point used 0.9.

A total of 9000 J/psis has been reconstructed in p+p 500GeV collisions with a signal significance of 58.6. In each p_T bins, we counted in the mass window of 2.7 $\sim$ 3.3 GeV/c^2, and subtracted all background(combinatorial and residual background), also correct the mass counting bias. The raw J/ψ spectra is shown in Figure 1.17.

7.2 Efficiency and acceptance correction

We obtained the J/ψ detection efficiency from the J/ψ embedding for BHT1 trigger. Since the input MC J/ψ p_T is a flat distribution, it may affect the final efficiency. We used an iteration method to get the final detection efficiency. A flat p_T distribution is used as an initial distribution. The final BHT1 J/ψ detection efficiency is shown in Figure 1.18.

8 J/ψ invariant p_T spectra

The J/ψ invariant p_T spectra is showed in Figure 1.19, The invariant p_T spectra is defined as:

$$B\frac{d^3N}{p_T dp_T dy d\phi} = \frac{1}{2\pi p_T}\frac{N_{J/\psi}}{\Delta p_T \Delta y \epsilon}$$

where $\Delta y = 2$ for $|y| < 1$, p_T is the mean transverse momentum in the $p_T$bin with width Δp_T and ϵ is the efficiency and acceptance correction. The J/ψ invariant X_T spectra is shown in Figure 1.20.

9 Systematic uncertainty on J/ψ p_T spectra measurement

The following sources has been taken into account in the systematic uncertainty evaluation: imperfect trigger simulation, imperfect tracking simulation, J/ψ yield extraction, as well as the nσ_e distribution.

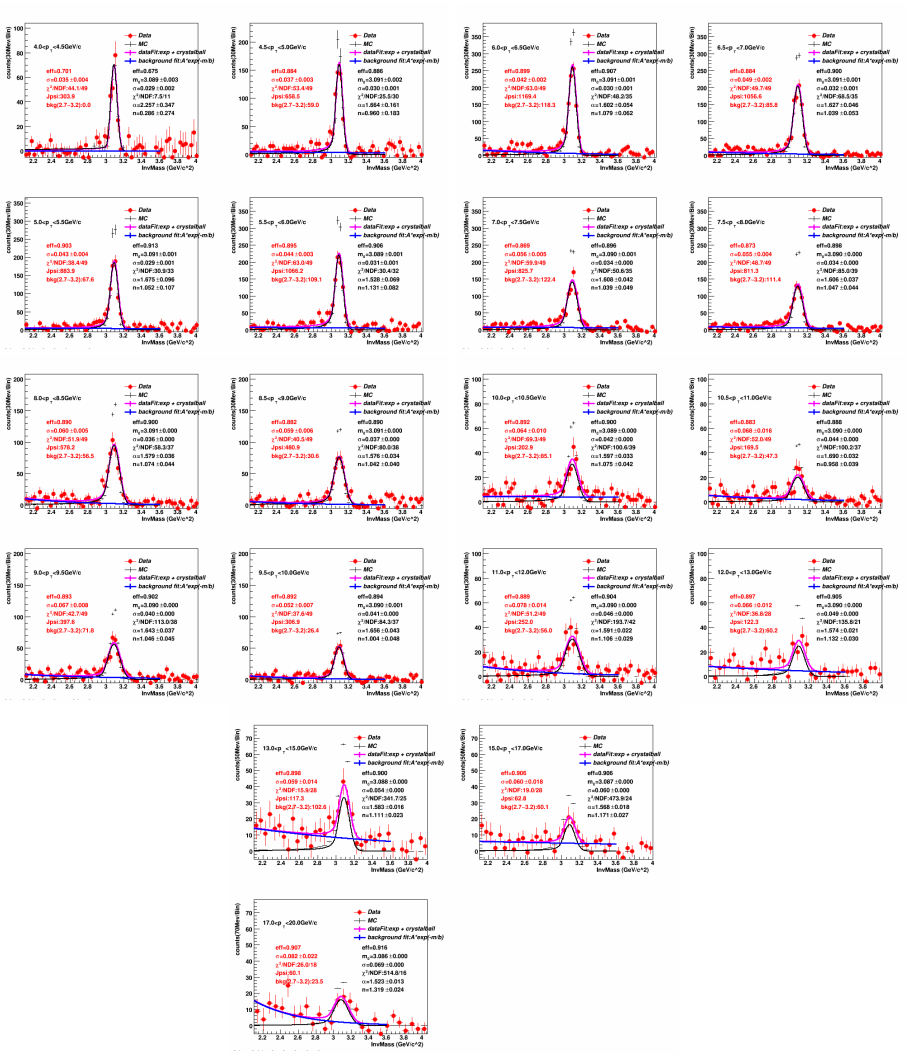

Figure 1.16: J/ψ yield extraction in each p_T bins

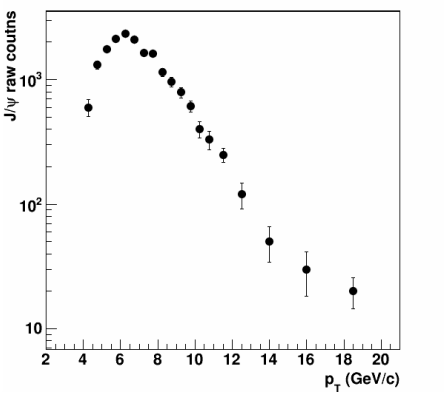

Figure 1.17: The raw J/ψ spectra.

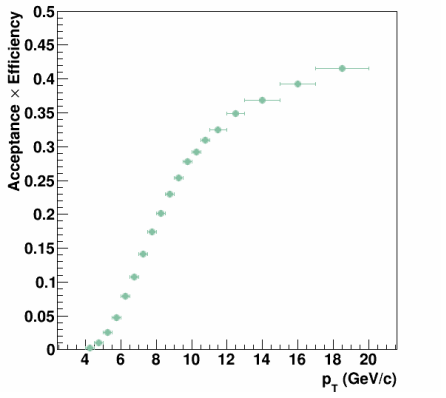

Figure 1.18: J/ψ Efficiency.

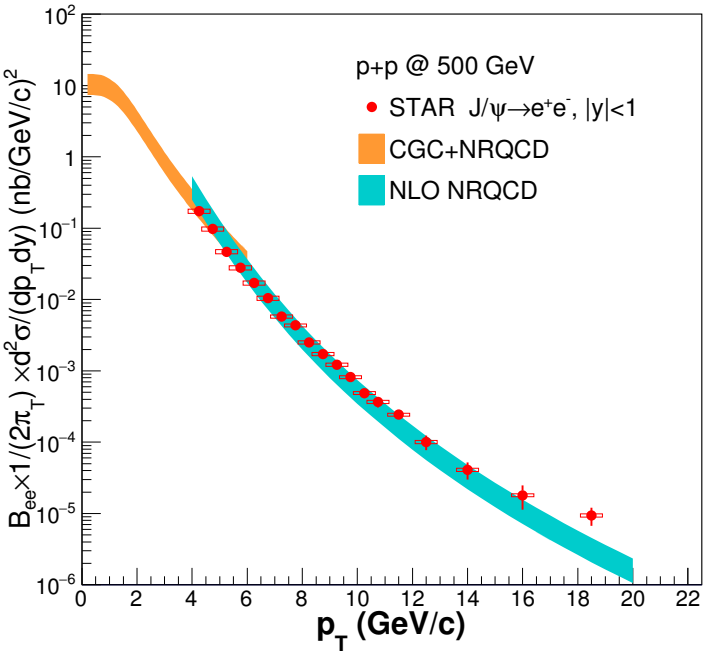

Figure 1.19: J/ψ p_T spectra

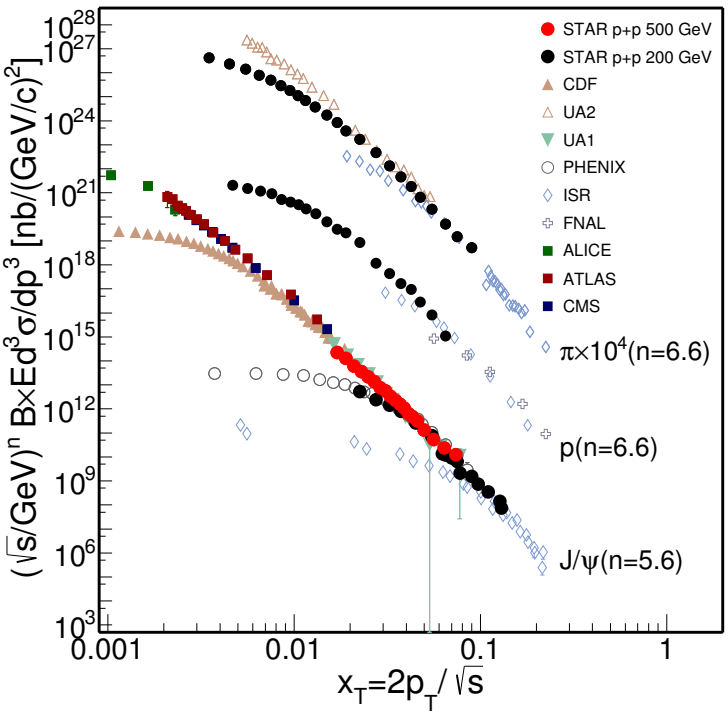

Figure 1.20: J/ψ x_T distribution

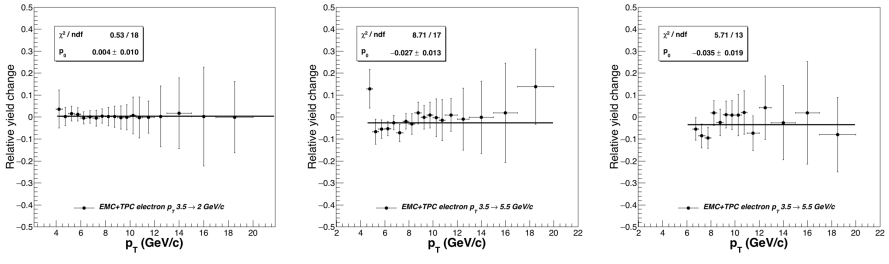

Figure 1.21: J/ψ bin-by-bin systematic uncertainties by varying p_T cut on "EMC+TPC" electron candidates.

The imperfect trigger simulation may caused by two reasons: imperfect momentum simulation and imperfect BEMC tower simulation. To estimate the imperfect momentum simulation, we changed the p_T cut of "EMC+TPC" electron candidates to 2 GeV/c, 4.5 GeV/c and 5.5 GeV/c, separately. By changing only on p_T cut in "EMC+TPC" electron candidates, the J/ψ raw yield and detection efficiency are recalculated and the difference between this two invariant yields is assigned as the systematic uncertainty. The bin by bin systematic uncertainty by varying p_T cuts on "EMC+TPC" electron candidates are shown in Figure 1.21. To average out the statistic fluctuation, a constant linear function is used to fit the bin-by-bin systematic uncertainties, the overall systematic uncertainties are 0.4%, 2.7% and 3.5% by using different p_T cuts. The maximum deviation is taken as the systematic uncertainty caused by p_T cuts.

We used the same method to evaluate the systematic uncertainty that originated from imperfect BEMC tower simulation by changing the adc0 value from 290 to 300. Another simulation related to BEMC is the pc/E cuts. pc/E cuts are important cuts to suppress the hadron in selecting "EMC+TPC" electron candidates. Different pc/E cuts for "EMC+TPC" electron candidates are used to estimate the systematic uncertainty from possible imperfect BEMC cluster response simulation in embedding. The adc0 cut contribute 0.5% in systematic uncertainty. The pc/E cuts contribute about 2.3% in total systematic uncertainty, as shown in Figure 1.22. The tracking efficiencies systematic uncertainty

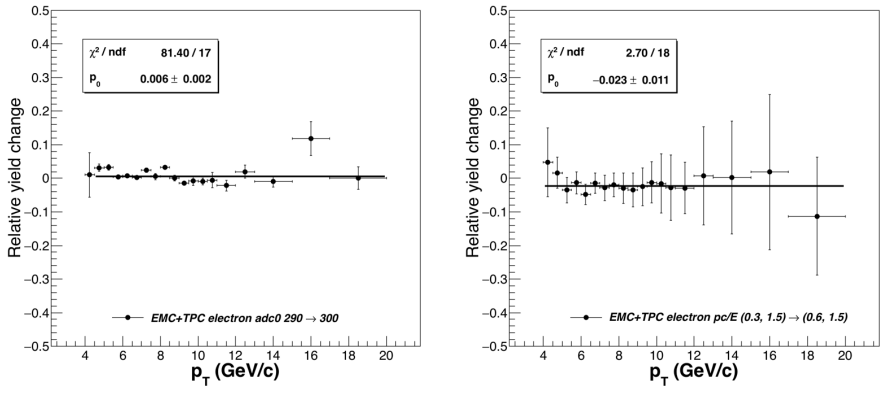

Figure 1.22: J/ψ bin-by-bin systematic uncertainties by varying adc0 cut and pcE cut on "EMC+TPC" electron candidates.

is studied by changing the "EMC + TPC" electron's DCA and "TPC" electron's DCA, respectively. The "EMC + TPC" electron candidate's DCA is changed from 1 cm to 2 cm and the "TPC" electron candidate's DCA is changed from 3 cm to 1 cm, as shown in Figure 1.23. The uncertainties associated with the

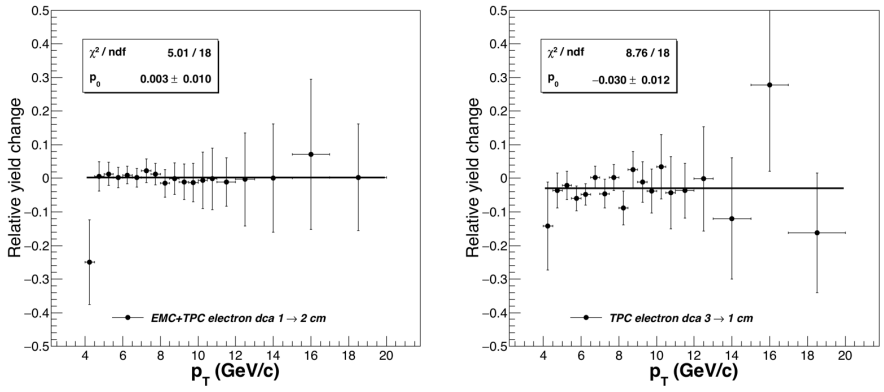

Figure 1.23: J/ψ bin-by-bin systematic uncertainties by varying "EMC+TPC" electron DCA cut and "TPC" electron DCA cut.

electron dE/dx identification efficiency is evaluate by change "EMC +TPC" and "TPC" electron's nσ_e cuts from (-2, 2) to (-2.5, 2.5), respectively, as shown in Figure 1.24.

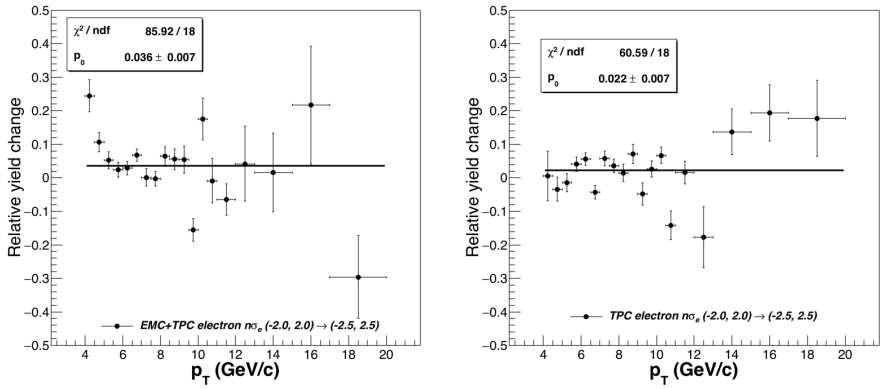

Figure 1.24: J/ψ bin-by-bin systematic uncertainties by varying "EMC+TPC" electron and "TPC" electron's nσ_e cuts.

Different mass counting range and fitting range are used to estimate the systematic uncertainties from yield extraction. We tried to enlarge and narrow down the signal counting mass range to evaluate the systematic uncertainties from mass counting range. The fitting range will affect residual background, we also enlarge and narrow down the fitting range to estimate systematic uncertainty from fitting process. The mass counting range and fitting range together contributes about 1.3% to the total systematic uncertainty.

The systematic uncertainties on J/ψ differential invariant cross-section are

Table 1.5: The summary of the systematic uncertainty in J/ψ p_T spectra

Source	systematic uncertainty
p_T	3.5%
$adc0$	0.5%
p/E	2.3%
DCA	3.0%
$n\sigma_e$	3.6%
yield extraction	1.3%
totoal	6.4%

summarized in Table 1.5 for BHT1 triggered data.

The J/ψ polarization parameter λ_θ is measured to be negative at high p_T region in proton-proton collisions at $\sqrt{s}$ = 200 GeV at STAR experiment [**?**]. The detector acceptance is different for different J/ψ polarization parameter. Hence, the J/ψ polarization is also a source of systematic uncertainty which affect the cross section measurement. Currently, there is no published J/ψ polarization measurement in p+p collisions at $\sqrt{s}$ = 500 GeV. STAR has a preliminary result on J/ψ polarization at $\sqrt{s}$ = 500 GeV with a p_T range of 5< p_T <16 GeV/c. We use this J/ψ polarization parameters to estimate the effect caused by polarization.

We assume that the polarization has a constant polarization parameter in the kinematic range of 0< p_T <5 GeV/c, which may over estimate the polarization parameter. We also assumed the polarization is the same with p_T large than 16 GeV/c. The J/ψ decay electron angular distribution will follow the distribution below:

$$dN/d\cos\theta \propto 1 + \lambda_\theta \cos^2(\theta) \tag{1.1}$$

The left panel of Figure 1.25 shows the J/ψ detection efficiency with and without polarization. The right panel shows the ratio of polarized J/ψ and unpolarized J/ψ efficiency difference, there is about 10% difference. The systematic uncertainty caused by J/ψ polarization is taken as a special systematic uncertainty as the efficiency enhancement can be primely addressed with more study on J/ψ polarization.

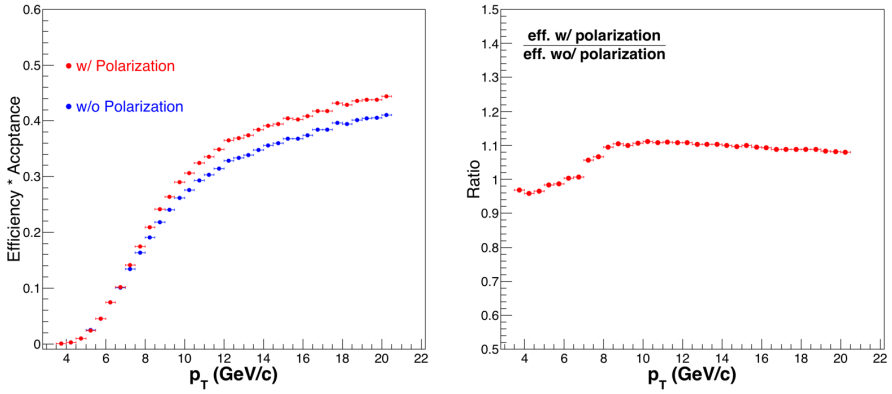

Figure 1.25: Left: J/ψ detection efficiency with (blue) and without (red) J/ψ polarization verse J/ψ p_T. Right: The ratio of J/ψ detection efficiency with and without J/ψ polarization.

Chapter 2

$\psi(2S)$ analysis

1 $\psi(2S)$ analysis

The data set used for the $\psi(2S)$ analysis is the same as used in the J/ψ analysis. Also, the online trigger is BHT1 trigger as used in the J/ψ analysis. The di-electron decay branch ratio for $\psi(2S)$ is $(7.72 \pm 0.17)\times10^{-3}$, which is about an order of magnitude lower than J/ψ. But due to the high enhancement of the electron rich sample in the BHT1 trigger events, we can still reconstruct the $\psi(2S)$ in the di-electron decay channel.

2 $\psi(2S)$ analysis detials

Since we are reconstructing the $\psi(2S)$ also in the di-electron channel by using the same data set and trigger just like in the J/ψ reconstruction. The vertex requirement of BHT1 events are a valid vertex and the reconstructed V_z should be inside the TPC. The primary requirement of J/ψ reconstruction is a very purity electron sample, which requires the electron fired the BHT1 trigger. Hence, in the $\psi(2S)$ analysis, we used the same method as in the J/ψ analysis. First, we selected the "EMC+TPC" electrons, then selected the "TPC" electrons. The selecting criteria are also the same as in the J/ψ analysis, which have been discussed in last section.

We pair the electron candidates and positron candidates from the same events to reconstruct the $\psi(2S)$ signal. The combinatorial background is estimated by the like-sign method as discussed in the J/ψ reconstruction. As for the residual background, we used a linear function to describe it. The yield extraction of $\psi(2S)$ method is by using bin counting, which counts the number of the count in the mass range of $3.5 < m_{inv} < 3.8$ GeV/c^2. The energy loss of the $\psi(2S)$ decayed electron is still there. Hence, a crystal ball function is

also employed to describe the reconstructed $\psi(2S)$ signal. The line shape of the $\psi(2S)$ is obtained from embedding technique as we have discussed in J/ψ analysis. Figure 2.1 shows the $\psi(2S)$ signals, the open circle is the raw signal, which is the unlike-sign signals minus the like-sign signals. The blue line shows the residual background. In this data sample, the $\psi(2S)$ signals are 305 $\pm$ 106 in the kinematics range of $4 < p_T < 12$ GeV/c. The signal strength is 3.9.

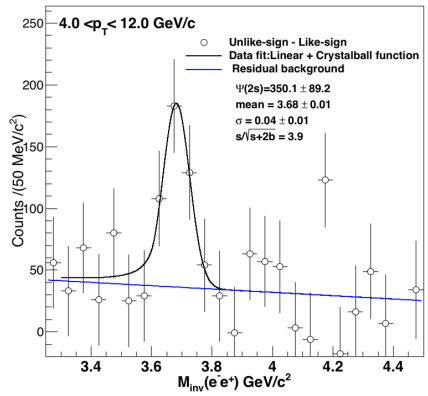

Figure 2.1: The $\psi(2S)$ signal after the combinatorial background subtraction (open black circles). Linear + Crystal ball function fitting are shown in black. Blue curve indicates the residual background.

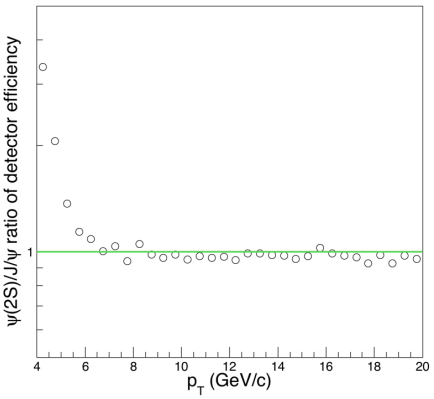

Figure 2.2: The detector efficiency difference between $\psi(2S)$ and J/ψ in the same BHT1 trigger events, $\psi(2S)$ are J/ψ are reconstructed by same selecting criterions on events, electron candidates.

In the $\psi(2s)$ analysis, we also required $\psi(2S)$ embedding sample, which embedded 5 $\psi(2S)$s in the real BHT1 data, with flat distributions in y, ϕ, as well as transverse momentum range of $0 < p_T < 20$ GeV/c. The $\psi(2S)$ transverse momentum shape is not measured in p+p collisions at $\sqrt{s} = 500$ GeV yet. As we have mentioned in the J/ψ measurement, we need a reasonable MC $\psi(2S)$ p_T shape, otherwise, the efficiency obtained from the embedding may not right. In this analysis, we assume that the $\psi(2S)$ has the same transverse momentum shape as J/ψ. With this assumption, we obtained the $\psi(2S)$ detector efficiency.

The total detector efficiency for $\psi(2S)$ may have some difference from J/ψ due to the different invariant mass. Figure 2.2 shows the $\psi(2S)$ efficiency to J/ψ efficiency ratio as a function of transverse momentum. The green line is a const function with y value equal to 1. A big difference can be found at the p_T about 4 GeV/c. In this p_T range, the energy of the decay electron, from both J/ψ and $\psi(2S)$, is near the trigger threshold ($\sim$ 4.3 GeV), and thus both have a low detector efficiency ($\sim$ 1%). Then one or two percent efficiency enhance will have a huge relative difference. The relative large invariant mass of $\psi(2S)$

can boost the decay electron to a higher energy. Thus, at about 4 GeV/c, the efficiency will have a huge difference. While at the high p_T range, the open angle between electron and positron from $\psi(2S)$ decay will slightly larger than J/ψ's in additional the trigger efficiency has been saturated at high-p_T. Hence, the main difference of detector efficiency for $\psi(2S)$ and J/ψ is the acceptance. A larger open angle means a smaller acceptance. Hence, at high p_T range the $\psi(2S)$ detector efficiency is slightly lower than the J/ψ.

3 $\psi(2S)$ to J/ψ yield ratio

The relative yields of $\psi(2S)$ to J/ψ mesons ratio is give by:

$$R = \frac{\frac{d^2\sigma}{dp_T dy}(\psi(2S)) \cdot \mathcal{B}(\psi(2S) \to e^+e^-)}{\frac{d^2\sigma}{dp_T dy}(J/\psi) \cdot \mathcal{B}(J/\psi \to e^+e^-)}. \tag{2.1}$$

Most of the systematic uncertainties from acceptance and efficiency correction are largely cancel out in the measurement. The $\psi(2S)$ is measured in the kinematic range of 4< p_T <12 GeV/c at mid-rapidity. The $\psi(2S)$ signal has been shown in Figure 2.1. The measured $\psi(2S)$ kinematic range is very large, it needs to think about where to place the data point. The same measurement with a large bin width will give very different physics information by placing the data point in different place in the bin. In this analysis, the data point is placed at the position where the yield coincides with the integrated yield of this bin. The $\psi(2S)$ yield shape has been assumed to be the same as J/ψ as discussed in analysis. The yield ratio is shown in Figure 2.3, the red bar shows the statistical uncertainty. The red box shows the systematic uncertainty.

The relative yield ratio of $\psi(2S)$ over J/ψ is 3.2 $\pm$ 1% in the kinematic range of 4< p_T <12 GeV/c. Here, the branch ratio is also included in the ratio measurement. The branch ratio of $\psi(2S) \to e^+e^-$ and $\psi(2S) \to e^+e^-$ branch ratio is (7.35 $\pm$ 0.18)$\times 10^{-3}$ and (5.94 $\pm$ 0.06)% respectively.

4 Systematic uncertainty on $\psi(2S)$ to J/ψ yield ratio measurement

The systematic uncertainty of $\psi(2S)$ to J/ψ yield ratio measurement are largely cancelled out due to the same set of cuts used in the analysis. In this analysis, the following uncertainties source are take into account: the p_T cuts of the triggered electron, the adc0 cut, the pc/E cuts, as well as the DCA value. The systematic uncertainty is extracted the same method as in J/ψ systematic

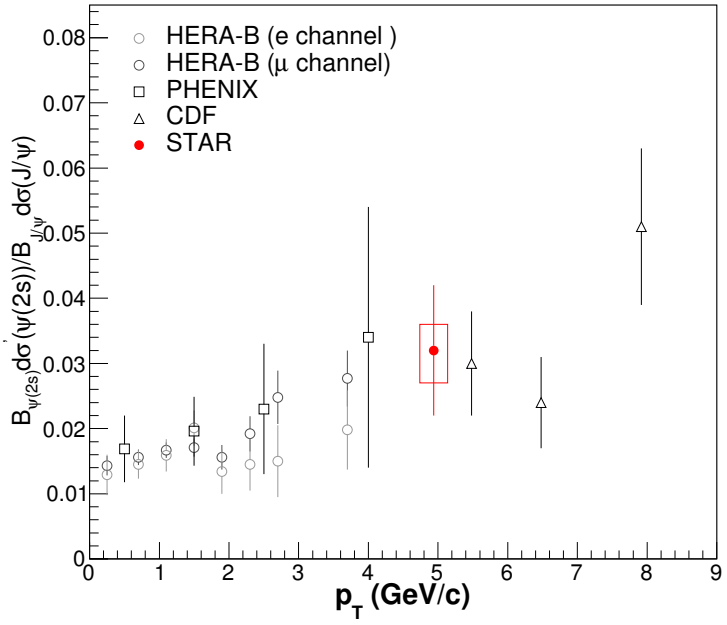

Figure 2.3: The relative yields of $\psi(2S)$ to J/ψ mesons. The kinematic range of this analysis is 4< p_T <12 GeV/c in the mid-rapidity of $|y|$ <1. The red error bar represents the statistical uncertainty. The red box represents the statistical uncertainties.

Table 2.1: The summary of the systematic uncertainty in $\psi(2S)$ p_T spectra

Source	systematic uncertainty
p_T	6.0%
$adc0$	3.0%
p/E	6.0%
DCA	3.0%
totoal	$< 11\%$

uncertainty study. The systematic uncertainties of $\psi(2S)$ to J/ψ yield ratio are summarized in Table 2.1. The total systematic uncertainty is less than 11%.